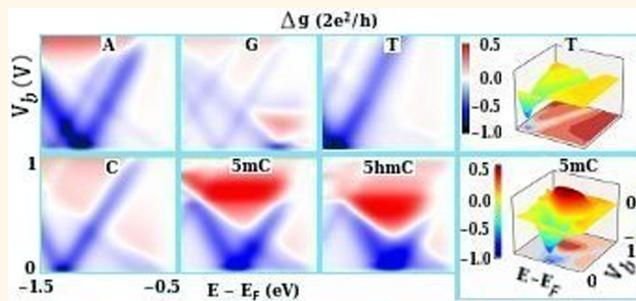


# Two Dimensional Molecular Electronics Spectroscopy for Molecular Fingerprinting, DNA Sequencing, and Cancerous DNA Recognition

Arunkumar Chitteth Rajan,<sup>†,‡</sup> Mohammad Reza Rezapour,<sup>‡,§</sup> Jeonghun Yun,<sup>†</sup> Yeonchoo Cho,<sup>†,\*</sup> Woo Jong Cho,<sup>†</sup> Seung Kyu Min,<sup>†</sup> Geunsik Lee,<sup>†</sup> and Kwang S. Kim<sup>†,‡,§,\*</sup>

<sup>†</sup>Department of Chemistry and <sup>‡</sup>Department of Physics, Pohang University of Science and Technology, Pohang 790-784, Korea, and <sup>§</sup>Department of Chemistry, Ulsan National Institute of Science and Technology (UNIST), Ulsan 689-798, Korea. <sup>†,‡,§</sup>Equal contribution.

**ABSTRACT** Laser-driven molecular spectroscopy of low spatial resolution is widely used, while electronic current-driven molecular spectroscopy of atomic scale resolution has been limited because currents provide only minimal information. However, electron transmission of a graphene nanoribbon on which a molecule is adsorbed shows molecular fingerprints of Fano resonances, *i.e.*, characteristic features of frontier orbitals and conformations of physisorbed molecules. Utilizing these resonance profiles, here we demonstrate two-dimensional molecular electronics spectroscopy



(2D MES). The differential conductance with respect to bias and gate voltages not only distinguishes different types of nucleobases for DNA sequencing but also recognizes methylated nucleobases which could be related to cancerous cell growth. This 2D MES could open an exciting field to recognize single molecule signatures at atomic resolution. The advantages of the 2D MES over the one-dimensional (1D) current analysis can be comparable to those of 2D NMR over 1D NMR analysis.

**KEYWORDS:** electron transport · Fano resonance · molecular electronics spectroscopy · DNA sequencing · methylated DNA

Molecular electronics<sup>1–6</sup> is a novel tool to investigate quantum transport phenomena. It can be utilized for third generation DNA sequencing using nanopores<sup>7–16</sup> and nanochannels.<sup>17</sup> Some nucleobases in DNA are frequently present in methylated form related to epigenetic modification to switch on/off the expression of genes or cancerous states. As such, methylated nucleobases<sup>18,19</sup> need to be recognized and differentiated from normal nucleobases. Nonetheless, molecular electronics is still in its infancy. Therefore, most molecular electronics approaches for sequencing proposed so far need to be drastically upgraded for practical implementation. As for single molecule spectroscopy and fast DNA sequencing at a level of atomic resolution, a new concept of Fano resonance driven 2D MES utilizing both bias and gate voltages can be exploited. This method is capable of

analyzing molecular fingerprints in the form of Fano resonances<sup>20–25</sup> from electron transmission, *viz.*, 2D conductance (high spatial resolution) instead of an optical or photonic approach (very low spatial resolution). To obtain such a Fano resonance of a molecule having discrete molecular orbital (MO) energy levels, graphene and graphene nanoribbon (GNR) are ideal materials with continuum band structure, since they show extraordinary electronic features for nanoelectronics.<sup>26–29</sup> It has been shown that nucleobases stacked on a GNR result in characteristic dips with sharp reductions in electronic transmission.<sup>17</sup> A narrow GNR providing few channels for ballistic<sup>30</sup> electron transport is considered as a quasi 1D system. In the recent past, the production of clean narrow GNRs has been an experimental hurdle. However, new advances have led to the molecular synthesis<sup>31,32</sup> and

\* Address correspondence to  
kimks@unist.ac.kr,  
fsdice@postech.ac.kr.

Received for review December 3, 2013  
and accepted January 21, 2014.

Published online January 21, 2014  
10.1021/nn4062148

© 2014 American Chemical Society

conductance measurements<sup>32,33</sup> of atomically precise defect free GNRs of width  $\sim 1$  nm.

Here we show Fano resonance-driven 2D MES by applying an external perturbation to a narrow armchair GNR (AGNR) which causes resonances in the corresponding electron transmission spectrum (Figure 1a). Once a certain molecule is attached on the AGNR surface, a ballistic electron transfer mode can be replaced by a new path of Fano resonance mode at a proper resonance condition. The transport characteristics of a molecule attached on the GNR surface strongly depend on the frontier MO energy levels and spatial orientations. Sharp dips/peaks in the transmission due to resonance with such MOs represent molecular fingerprints and reflect molecular configurations. Thus, the characteristic dips in the electron transmission at both electron channel energies ( $E - E_F$  where  $E_F$  is the Fermi energy) and bias voltages ( $V_b$ ) can be exploited for the 2D MES.

The 2D MES should be useful for single molecule spectroscopy at atomic resolution based on Fano resonance driven molecular fingerprinting and conformational analysis, while widely used laser driven molecular spectroscopy suffers from low resolution due to the diffraction limit of light wave. This single molecule recognition can be further utilized to distinguish different types of nucleobases for fast DNA sequencing without highly time-consuming complicated chemical/optical labeling procedure. It should be

noted that some nucleobases in DNA are frequently present in methylated form. The most dramatic consequence of DNA methylation would be cancer. Hence, recognition of methylated bases could give a precancer warning sign. Since methylation alters the energy levels and coupling strengths of MOs, the 2D MES utilizing Fano resonance should be able to distinguish methylated nucleobases from normal nucleobases. Hence, this method would have a great advantage over the available methylated DNA detection such as bisulfite treatment and amplification.<sup>18</sup>

## RESULTS AND DISCUSSION

The first step toward experimental implementation of such devices is to identify a single molecule on a GNR. As such, we apply an external perturbation by introducing a naphthalene molecule onto 10-AGNR (Figure 1). For simplicity, 10-AGNR will be simply denoted as AGNR unless otherwise specified. The molecule is stacked in the middle of the AGNR at a distance of 3 Å (this conformation is arbitrarily chosen). Due to the orbital overlap between the molecule and AGNR, a dip occurs in the electron transmission of AGNR with respect to  $E - E_F$  which can be controlled by the gate voltage ( $V_g$ ) (see the Methods section). The transmission ( $\tau$ ) curve shows a nearly symmetric dip at  $-1.2$  eV. Since  $\pi-\pi$  stacking<sup>34</sup> is responsible for the noncovalent interaction<sup>35</sup> between naphthalene and AGNR, the resulting coupling gives a large width of the transmission reduction by one quanta, as can be understood from the density of states (DOS). As the distance between molecule and AGNR increases, the resulting weaker coupling decreases the width of the transmission reduction.<sup>36,37</sup> However, the coupling strength does not change significantly for the tilting angles less than  $10^\circ$  at a stacking distance  $d$  of  $\sim 3.0$ – $3.5$  Å due to the  $\pi-\pi$  interaction.<sup>38–40</sup> Figure 1a depicts the transmission reduction caused by the naphthalene molecule stacked on the AGNR surface ( $d = 3$  Å) as a single Fano resonance in the Fano-Anderson model (Figure 1c,d).<sup>21</sup> Cytosine on a parallel stacked configuration on an AGNR produces overlapped double Fano resonance due to the nearly degenerate levels of its highest occupied MOs (HOMOs). Likewise, any other molecule, upon an external perturbation, uniquely contributes to the AGNR transmission, revealing the characteristic fingerprint and conformation of an individual molecule.

We consider the three systems of (i) P, pristine-AGNR and (ii/iii) N/T, naphthalene/thymine physisorbed on an AGNR ( $d = 3$  Å). Figure 2 shows the 2D conductance features depending on both  $E - E_F$  and  $V_b$ , in contrast to the 1D current ( $I$ ) feature depending on  $V_b$ . The plot of transmission  $\tau$  vs  $E - E_F$  at varying  $V_b$  clearly distinguishes different molecules by their molecular fingerprints (Figure 2a). Therefore, once the relative differential conductance ( $\Delta g$  with respect to the

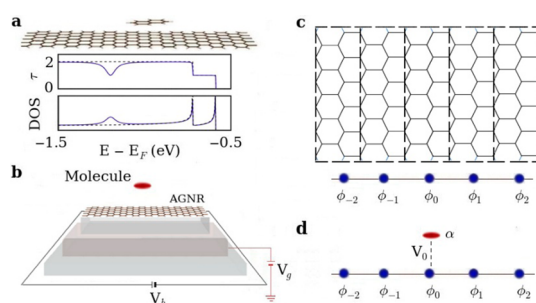


**Figure 1.** Fano resonance dip. (a) Electron transmissions ( $\tau$ ) and DOSs against electron channel energy ( $E - E_F$ ) for the pristine (dotted line) vs naphthalene adsorbed (solid line) 10-AGNR (composed of 10 parallel C–C bonds within the AGNR width). The dangling bonds are hydrogen-terminated. (b) A schematic of electronic current and conductance measurements of an adsorbed molecule. (c) Fano-Anderson model<sup>21</sup> for AGNR. Each box stands for a unit cell of graphene, which is symbolized by a circle in a linear chain.<sup>24,50</sup> (d) Schematic representation of the Fano-Anderson configuration. An adsorbed molecule (brown oval) has discrete quantum states, while AGNR is a quasi one-dimensional structure. The concept of this transport system can be understood from an approximate model Hamiltonian:  $H = \sum_n C\phi_n\phi_{n-1}^\dagger + \varepsilon_\alpha|\alpha|^2 + \alpha^\dagger \sum_j V_j\phi_j + c.c.$ , where  $\phi_n$  is the Bloch wave at site  $n$ , coupled by a nearest neighbor hopping parameter  $C$  in a chain.  $\varepsilon_\alpha$  is the energy of state  $\alpha$  belonging to the molecule and  $V_j$  is the coupling strength between site  $j$  and state  $\alpha$ . The first term in the equation describes the interaction between sites in the chain. This solution explains the symmetric transmission dip in Figure panel a (Supporting Information).

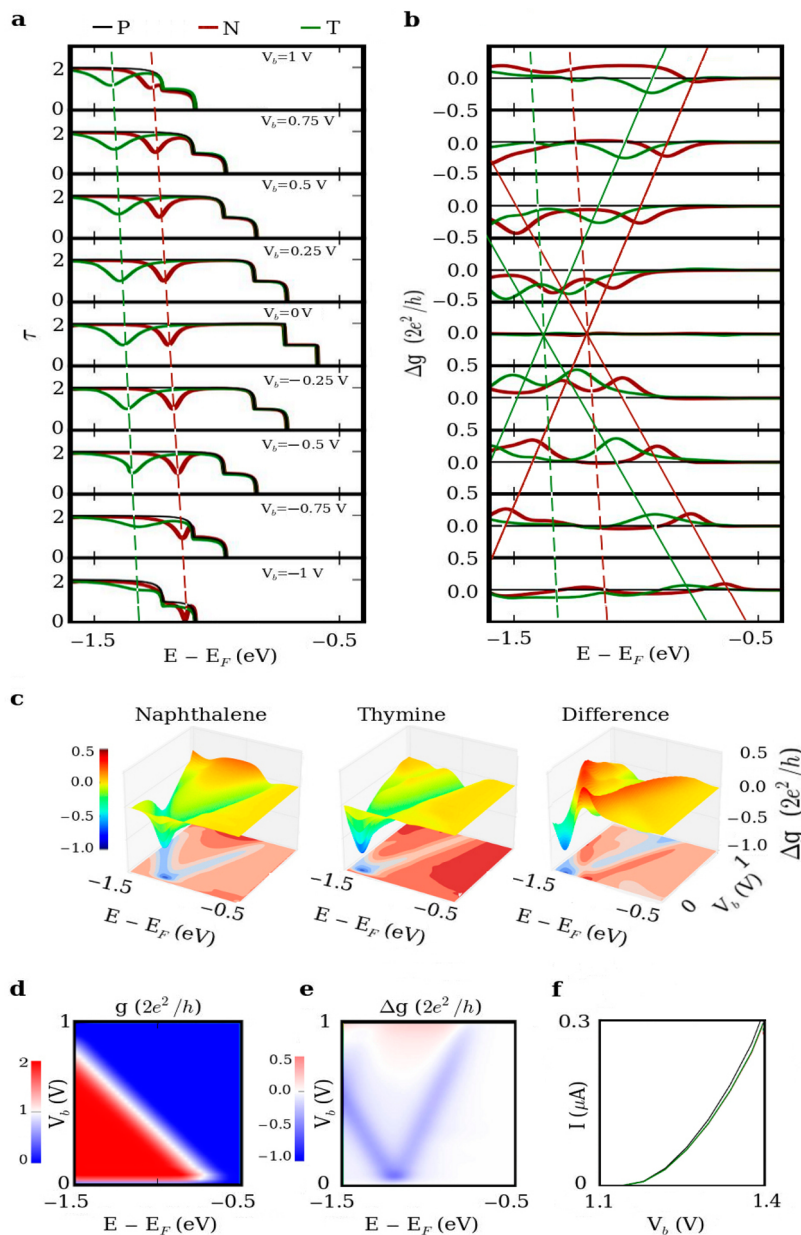


**Figure 2.** 2D transmission and differential conductance maps. (a–c) Transmission  $\tau$  (a) and relative differential conductance  $\Delta g$  ((b) 2D view; (c) 3D view) with respect to electron channel energies ( $E - E_F$ ) at varying bias voltages  $V_b$  for pristine-AGNR (P; in black), naphthalene (N; in brown) or thymine (T; in green) stacked on 10-AGNR. (d) Differential conductance  $g$  for P. (e)  $\Delta g$  for N. (f) 1D current ( $I$ ) at varying  $V_b$ .

pristine-AGNR, where the differential conductance is  $g = dI/dV_b$  is measured at varying  $V_b$  and  $E - E_F$ , the distinction between naphthalene and thymine becomes clear (2D and 3-dimensional (3D) views in Figure 2, panels b and c, respectively). For visual aids, the  $g$  of the pristine-AGNR (P) and  $\Delta g$  of the naphthalene-AGNR (N) are shown in Figure 2, panels d and e, respectively.

When  $V_b$  is applied, the transmission gap shown along  $E - E_F$  widens almost linearly against  $V_b$  because the chemical potentials of source and drain electrodes with a band gap are changed by  $\pm V_b/2$ . The response of local electron density of the adsorbed molecule is

observed in terms of the transmission dip, which can be recognized by controlling  $V_g$ . Thus, 2D conductance spectroscopy can be utilized to recognize the molecular species stacked on an AGNR. As  $V_b$  increases, the dip in  $\tau$  shifts with almost a constant slope, which arises from the linear dipole moment-driven Stark effect reflecting the MOs responsible for resonance dips in  $\tau$  (Figure 2a, Supporting Information Figure S1). At  $V_b = 0$ , the dip in  $\tau$  is far from the band edge. However, as  $|V_b|$  increases, the band edge appears at a more negative value of  $E - E_F$ , approaching to the dip. This makes the measurement of  $g$  practical because the Fano dips can be measured without applying high gate

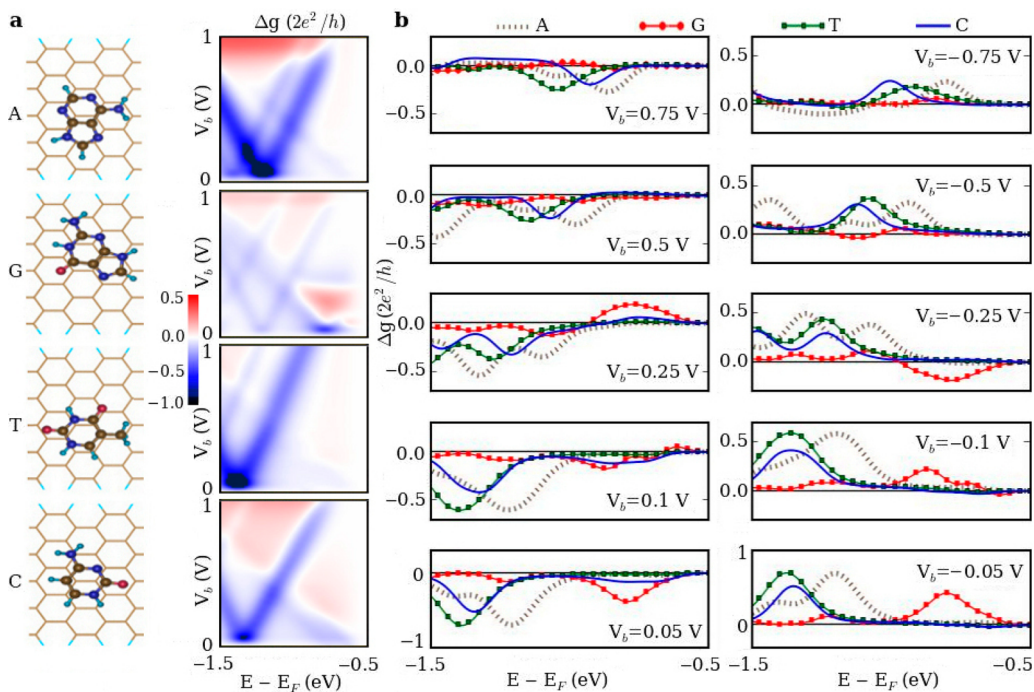


**Figure 3.** 2D relative differential conductance maps for nucleobases A, G, T, and C. (a) Stacked structures on AGNR and 2D  $\Delta g$  maps at varying electron channel energy  $E - E_F$  and bias voltage  $V_b$  for each nucleobase. (b) Characteristic dips/peaks in  $\Delta g$  for the nucleobases at varying  $V_b$ .

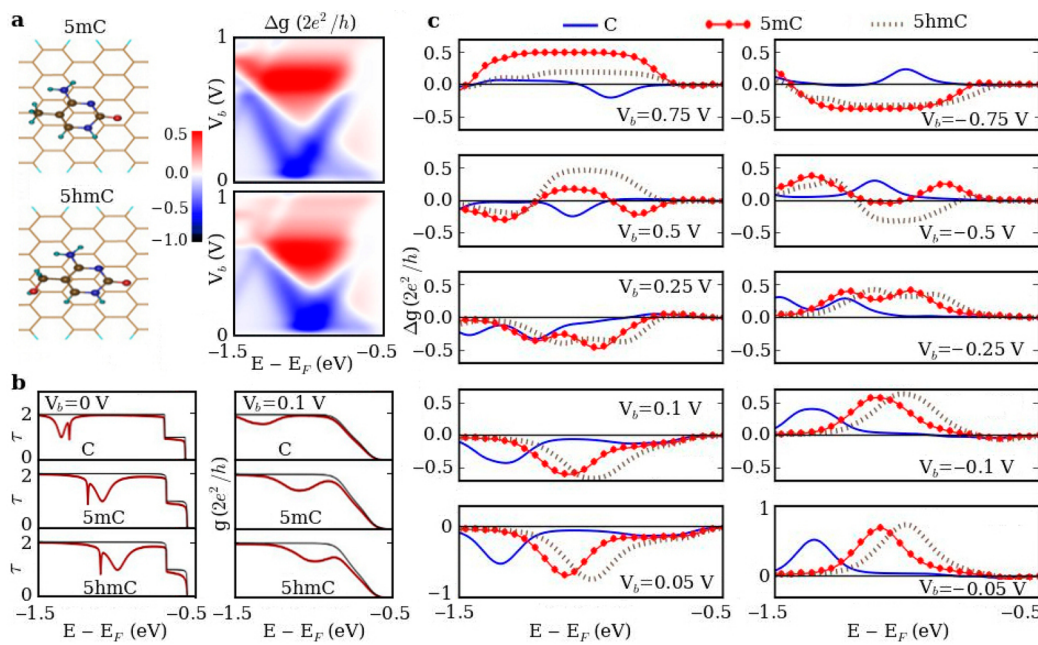
voltage. Then, for the given  $V_b$ , the  $g$  also gives a weak dip at the  $E - E_F$  which shifts by almost the same amount of the energy difference in  $E - E_F$  from the band edge to the dip in  $\tau$ . The  $\Delta g$  shows such energy shifts in  $E - E_F$  along both positive and negative directions, because the differential of a dip gives both positive and negative slopes, giving an X-shape dips pattern in the 2D map for  $-1 \text{ V} < V_b < 1 \text{ V}$  (Figure 2b). The 2D plot of  $\Delta g$  with respect to  $V_b$  and  $E - E_F$  shows the differences in characteristic features between different molecules as noted in Figure 2b,c, in contrast to the 1D plot of  $I$  vs  $V_b$  which hardly distinguishes different molecules as in Figure 2f. This is the reason why the 2D MES can clearly recognize the molecular fingerprints, while the 1D current measurement cannot provide any useful information of molecules.

Figure 3 shows the 2D relative differential conductance  $\Delta g$  of the four different types of nucleobases (A, C, G, T) at the geometry reported in a previous work.<sup>17</sup> The position and change of  $\Delta g$  for each nucleobase is different. This distinction is more visible at the selected  $V_b$ 's (Figure 3b). The dips/peaks at  $E - E_F$  shift according to  $V_b$ , as noted in the 2D maps showing the Fano resonance behavior in the corresponding transmission spectrum of the nucleobases. For example, at  $V_b = 0.05 \text{ V}$ , the G can be easily recognized from a dip at  $E - E_F = -0.79 \text{ eV}$ , while the A/C/T, from a dip at  $-1.21/-1.34/-1.39 \text{ eV}$ . At  $V_b = 0.75 \text{ V}$ , the A/C/T dip appears at  $-0.86/-0.93/-1.04 \text{ eV}$ , while at  $V_b = -0.75 \text{ V}$ , the A/C/T dip is at  $-0.80/-1.01/-0.92 \text{ eV}$ . In this way, the 2D  $\Delta g$  map distinguishes the different types of

nucleobases. For practical use, variations of 2D spectral maps depending on molecules and conformations can be stored in a database. Then, through data search and analysis, the characterization of a molecule including species and conformation would be possible using the obtained 2D relative differential conductance spectroscopy data. In the case of very fast moving molecules, a less sensitive 2D  $\Delta g'$  ( $= I/V_b$  instead of  $dI/dV_b$ ) map could be used.

In Figure 4, the transmission  $\tau$  distinguishes between C, 5-methylcytosine (5mC), and 5-hydroxymethylcytosine (5hmC). For practical measurements, the  $\Delta g$  can be used. For example, at  $V_b = 0.5 \text{ V}$ , two dips at  $E - E_F = -1.07$  and  $-0.82 \text{ eV}$  and one peak around  $-1.02 \text{ eV}$  correspond to the three different types of cytosine nucleobases, respectively. The dips/peaks of  $\Delta g$  along  $E - E_F$  at varying  $V_b$  show the characteristic differences between methylated and unmethylated nucleobases. This simple method would show a great advantage over the commonly used bisulfite treatment and amplification method<sup>18</sup> currently used in precancer tests for recognizing methylated nucleobases.

The effects of both width and edge disorders of AGNR on the Fano resonance are given in Supporting Information Figure S2. We note that the validity of applying the Fano-Anderson model to the molecule-AGNR system for molecular sensing holds irrespective of the width of AGNR. However, as the width increases, the resulting increase in the number of transmission channels within a given energy window gives less



**Figure 4.** 2D relative differential conductance maps for methylated nucleobases. (a) Stacked structures on AGNR and 2D  $\Delta g$  maps for varying  $E - E_F$  and  $V_b$  for methylated cytosine nucleobases (5mC, 5hmC). (b and c) Characteristic dips/peaks in  $\tau$  and  $g$  (b) and those in  $\Delta g$  (c) at varying  $V_b$  for C, 5mC, and 5hmC.

distinctive Fano resonance dips. Since the defect free narrow GNRs can be chemically synthesized, it is not necessary to consider the AGNR systems with defects. Nevertheless, it is interesting to investigate the Fano resonance phenomena in such defective systems, because first principle studies show that the presence of disorders in GNRs can adversely affect their properties.<sup>41</sup> We investigated the resonance effects using AGNRs with two extra hexagonal-rings and an extra-pentagon ring on its boundary and a naphthalene molecule stacked on such a defected AGNR surface. Though the presence of edge disorders give slight shifts in Fano dips, the key characteristic features of the molecule are still kept, and so the Fano dips can be re-referenced for the given defect system.

Controlling the bias voltage is a useful means to extend and enrich spectroscopic observables. For well stacked conformations with similar orientations, as in simulations of DNA in a nanochannel, the nucleobases on GNR can be differentiated without significant overlaps between different types of nucleobases. However, if conformational changes are large, conformation-dependent changes in Fano dips can be utilized for conformational analysis. Namely, (i) either if it is known which nucleobase is on GNR or (ii) if 2D (or 1D) conductance spectrum is mapped to previously built database, the conformation can be identified. On the basis of the bias-dependent transmission data, the Stark shifts observed from Fano dips that they change nearly linearly to the applied  $V_b$  reflect that they are originated from the linear Stark effect<sup>42</sup> (almost proportional to the dipole moment component of the resonance MO) (Figure 2a). Then, the orientation of a

nucleobase on GNR could be identified, without resorting to complex mapping to fingerprints. Once we know the dip position at finite biases, the dip position could be inferred at the zero bias. Another advantage of applying the bias voltage is that the gate voltage required to observe Fano dips can be much reduced due to the band gap of the semiconducting property of AGNR. In this regard, DNA sequencing and DNA methylation recognition would be more realistic when both the bias and gate voltages are controlled.

In practical measurements, gate voltage sweep needs to be performed for each bias voltage. The time required for measurements is the number of the selected bias voltages times the time for a gate voltage sweep. However, to distinguish nucleobases, not many bias voltages are necessary; only measurements at two or three different bias voltages would be sufficient, as can be seen from Figures 3 and 4. Thus, the time required for reliable measurements is a similar order of magnitude to the case when the bias voltage is not controlled. Also the structural fluctuation due to temperature needs to be considered. Our design exploits the strong  $\pi-\pi$  stacking interaction which minimizes structural fluctuations. Additionally, when a nucleobase is connected to the main strand, rotational motion is significantly restricted. Therefore, fluctuation of the nucleobase is small, and transmission does not change significantly. Nevertheless, at room temperature nucleobases experience some fluctuations in their configuration on the AGNR surface, while they remain mostly in the middle of AGNR. The four different types of nucleobases still exhibit their characteristic features, differentiating different nucleobases. The

2D conductance map reflecting varying bias voltages would allow the four types of nucleobases to be differentiated (Supporting Information).

## CONCLUSIONS

In summary, we demonstrate that a 2D conductance spectrum is capable of identifying single molecules and their conformation. The spectrum is obtained by controlling both bias and gate voltages applied to an AGNR. A stacked molecule generates a characteristic

spectrum representing electronic level and coupling due to Fano resonance. Variations of the 2D  $\Delta g$  maps depending on specific molecules and conformations can be stored as a database. In this way, the characteristic 2D differential conductance maps can be utilized to recognize adsorbed molecules and their conformations. This could open an exciting new field of Fano resonance driven 2D MES, which should hold similar advantages like 2D NMR over 1D NMR spectroscopy.

## METHODS

We perform the transport calculations based on density functional theory (DFT) with single-particle Green's function method.<sup>43–45</sup> The transmission is given by,

$$\tau = \text{Tr}[\Gamma_L G \Gamma_R G^\dagger]$$

where Tr represents the trace,  $\Gamma_{L/R} = i[\Sigma_{L/R} - \Sigma_{L/R}^\dagger]$  with  $\Sigma_{L/R}$  as the self-energy of the left/right electrode and  $G$  denotes the Green's function. The Landauer-Büttiker formalism is utilized to calculate the current:

$$I(E_F, V_b) = \frac{2e}{h} \int \tau(E, V_b) [f(E, \mu_s) - f(E, \mu_d)] dE$$

where  $\mu_{s/d} = E_F \pm V_b/2$ .  $E_F$  changes on the application of  $V_g$ , which means the virtual sweeping of  $[f(E, \mu_s) - f(E, \mu_d)]$  to the given energy point. To treat the exchange-correlation effects, we employ the Ceperley-Alder form as parametrized by Perdew and Zunger<sup>46</sup> in the local density approximation (LDA). The double- $\zeta$  polarization basis set and the Troullier-Martins pseudopotential<sup>47</sup> and 500 Ry cutoff energy for the grid-mesh are employed in the calculations. The transport calculations are accomplished with the PosTrans code<sup>29,48</sup> plugged into the Siesta package.<sup>49</sup> The dangling bonds are hydrogen-terminated.

*Conflict of Interest:* The authors declare no competing financial interest.

*Acknowledgment.* This work was supported by NRF (National Honor Scientist Program: 2010-0020414) and KISTI (KSC-2011-G3-02).

*Supporting Information Available:* Additional data including Fano-Anderson model, Figures S1–S4 and a table. This material is available free of charge via the Internet at <http://pubs.acs.org>.

## REFERENCES AND NOTES

- Ratner, M. A Brief History of Molecular Electronics. *Nat. Nanotechnol.* **2013**, *8*, 378–381.
- Song, H.; Kim, Y.; Jang, H.-W.; Jeong, H.; Reed, M. A.; Lee, T. Observation of Molecular Orbital Gating. *Nature* **2009**, *462*, 1039–1043.
- Cuniberti, G.; Fagas, G.; Richter, K. *Introducing Molecular Electronics*; Springer: New York, 2005.
- Kim, W. Y.; Choi, Y. C.; Min, S. K.; Cho, Y.; Kim, K. S. Application of Quantum Chemistry to Nanotechnology: Electron and Spin Transport in Molecular Devices. *Chem. Soc. Rev.* **2009**, *38*, 2319–2333.
- Cho, W. J.; Cho, Y.; Min, S. K.; Kim, W. Y.; Kim, K. S. Chromium Porphyrin Arrays as Spintronic Devices. *J. Am. Chem. Soc.* **2011**, *133*, 9364–9369.
- Shen, L.; Zeng, M.; Yang, S. W.; Zhang, C.; Wang, X.; Feng, Y. Electron Transport Properties of Atomic Carbon Nanowires Between Graphene Electrodes. *J. Am. Chem. Soc.* **2010**, *132*, 11481–11486.
- Shendure, J.; Ji, H. Next-Generation DNA Sequencing. *Nat. Biotechnol.* **2008**, *26*, 1135–1145.
- Huang, S.; He, J.; Chang, S.; Zhang, P.; Liang, F.; Li, S.; Tuchband, M.; Fuhrmann, A.; Ros, R.; Lindsay, S. Identifying Single Bases in a DNA Oligomer with Electron Tunnelling. *Nat. Nanotechnol.* **2010**, *5*, 868–873.
- Tsutsui, M.; Taniguchi, M.; Yokota, K.; Kawai, T. Identifying Single Nucleotides by Tunnelling Current. *Nat. Nanotechnol.* **2010**, *5*, 286–290.
- Prasongkit, J.; Grigoriev, A.; Pathak, B.; Ahuja, R.; Scheicher, R. H. Transverse Conductance of DNA Nucleotides in a Graphene Nanogap from First Principles. *Nano Lett.* **2011**, *11*, 1941–1945.
- Scheicher, R. H.; Grigoriev, A.; Ahuja, R. DNA Sequencing with Nanopores from an *ab Initio* Perspective. *J. Mater. Sci.* **2012**, *47*, 7439–7446.
- Ahmed, T.; Kilina, S.; Das, T.; Haraldsen, J. T.; Rehr, J. J.; Balatsky, A. V. Electronic Fingerprints of DNA Bases on Graphene. *Nano Lett.* **2012**, *12*, 927–931.
- Nelson, T.; Zhang, B.; Prezhdo, O. V. Detection of Nucleic Acids with Graphene Nanopores: *Ab Initio* Characterization of a Novel Sequencing Device. *Nano Lett.* **2010**, *10*, 3237–3242.
- Saha, K. K.; Drndić, M.; Nikolić, B. K. DNA Base-Specific Modulation of Microampere Transverse Edge Currents through a Metallic Graphene Nanoribbon with a Nanopore. *Nano Lett.* **2012**, *12*, 50–55.
- Zwolak, M.; Di Ventra, M. Colloquium: Physical Approaches to DNA Sequencing and Detection. *Rev. Mod. Phys.* **2008**, *80*, 141–165.
- Lagerqvist, J.; Zwolak, M.; Di Ventra, M. Fast DNA Sequencing via Transverse Electronic Transport. *Nano Lett.* **2006**, *6*, 779–782.
- Min, S. K.; Kim, W. Y.; Cho, Y.; Kim, K. S. Fast DNA Sequencing with a Graphene Based Nanochannel Device. *Nat. Nanotechnol.* **2011**, *6*, 162–165.
- Jaenisch, R.; Bird, A. Epigenetic Regulation of Gene Expression: How the Genome Integrates Intrinsic and Environmental Signals. *Nat. Genet.* **2003**, *33*, 245–254.
- Clark, S. J.; Statham, A.; Stirzaker, C.; Molloy, P. L.; Frommer, M. DNA Methylation: Bisulphite Modification and Analysis. *Nat. Protoc.* **2006**, *1*, 2353–2364.
- Fano, U. Effects of Configuration Interaction on Intensities and Phase Shifts. *Phys. Rev.* **1961**, *124*, 1866–1878.
- Miroshnichenko, A. E.; Flach, S.; Kivshar, Y. S. Fano Resonances in Nanoscale Structures. *Rev. Mod. Phys.* **2010**, *82*, 2257–2298.
- Fan, S.; Suh, W.; Joannopoulos, J. D. Temporal Coupled-Mode Theory for the Fano Resonance in Optical Resonators. *J. Opt. Soc. Am. A* **2003**, *20*, 569–572.
- Kim, J.; Kim, J.-R.; Lee, J.-O.; Park, J. W.; So, H. M.; Kim, N.; Kang, K.; Yoo, K.-H.; Kim, J.-J. Fano Resonance in Crossed Carbon Nanotubes. *Phys. Rev. Lett.* **2003**, *90*, 166403.
- Miroshnichenko, A. E.; Mingaleev, S. F.; Flach, S.; Kivshar, Y. S. Nonlinear Fano Resonance and Bistable Wave Transmission. *Phys. Rev. E* **2005**, *71*, 036626.
- Sasaki, S.; Tamura, H.; Akazaki, T.; Fujisawa, T. Fano-Kondo Interplay in a Side Coupled Double Quantum Dot. *Phys. Rev. Lett.* **2009**, *103*, 266806.

26. K. S. Novoselov, K. S.; Geim, A. K.; Morozov, S. V.; Jiang, D.; Zhang, Y.; Dubonos, S. V.; Grigorieva, I. V.; Firsov, A. A. Electric Field Effect in Atomically Thin Carbon Film. *Science* **2004**, *306*, 666–669.
27. Kim, K. S.; Zhao, Y.; Jang, H.; Lee, S. Y.; Kim, J. M.; Kim, K. S.; Ahn, J.-H.; Kim, P.; Choi, J.-Y.; Hong, B. H. Large-Scale Pattern Growth of Graphene Films for Stretchable Transparent Electrodes. *Nature* **2009**, *457*, 706–710.
28. Son, Y.-W.; Cohen, M. L.; Louie, S. G. Half-Metallic Graphene Nanoribbons. *Nature* **2006**, *444*, 347–349.
29. Kim, W. Y.; Kim, K. S. Prediction of Very Large Values of Magnetoresistance in a Graphene Nanoribbon Device. *Nat. Nanotechnol.* **2008**, *3*, 408–412.
30. Tworzydlo, J.; Trauzettel, B.; Titov, M.; Rycerz, A.; Beenakker, C. W. J. Sub-Poissonian Shot Noise in Graphene. *Phys. Rev. Lett.* **2006**, *96*, 246802.
31. Cai, J.; Ruffieux, P.; Jaafar, R.; Bieri, M.; Braun, T.; Blankenburg, S.; Muoth, M.; Seitsonen, A. P.; Saleh, M.; Feng, X.; et al. Atomically Precise Bottom-Up Fabrication of Graphene Nanoribbons. *Nature* **2010**, *466*, 470–473.
32. Chen, Y.-C.; Oteyza, D. G. d.; Pedramrazi, Z.; Chen, C.; Fischer, F. R.; Crommie, M. F. Tuning the Band Gap of Graphene Nanoribbons Synthesized from Molecular Precursors. *ACS Nano* **2013**, *7*, 6123–6128.
33. Koch, M.; Ample, F.; Joachim, C.; Grill, L. Voltage-Dependent Conductance of a Single Graphene Nanoribbon. *Nat. Nanotechnol.* **2012**, *7*, 713–717.
34. Kim, K. S.; Tarakeshwar, P.; Lee, J. Y. Molecular Clusters of  $\pi$ -Systems: Theoretical Studies of Structures, Spectra, and Origin of Interaction Energies. *Chem. Rev.* **2000**, *100*, 4145–4186.
35. Georgakilas, V.; Otyepka, M.; Bourlinos, A. B.; Chandra, V.; Kim, N.; Kemp, K. C.; Hobza, P.; Zboril, R.; Kim, K. S. Functionalization of Graphene: Covalent and Non-covalent Approaches, Derivatives and Applications. *Chem. Rev.* **2012**, *112*, 6156–6214.
36. Cho, Y.; Min, S. K.; Kim, W. Y.; Kim, K. S. The Origin of Dips for the Graphene-Based DNA Sequencing Device. *Phys. Chem. Chem. Phys.* **2011**, *13*, 14293–14296.
37. Kim, W. Y.; Kim, K. S. Tuning Molecular Orbitals in Molecular Electronics and Spintronics. *Acc. Chem. Res.* **2010**, *43*, 111–120.
38. Meng, S.; Maragakis, P.; Papaloukas, C.; Kaxiras, E. DNA Nucleoside Interaction and Identification with Carbon Nanotubes. *Nano Lett.* **2007**, *7*, 45–50.
39. Cho, Y.; Min, S. K.; Yun, J.; Kim, W. Y.; Tkatchenko, A.; Kim, K. S. Noncovalent Interactions of DNA Bases with Naphthalene and Graphene. *J. Chem. Theory Comput.* **2013**, *9*, 2090–2096.
40. Lee, J.-H.; Choi, Y.-K.; Kim, H.-J.; Scheicher, R. H.; Cho, J.-H. Physisorption of DNA Nucleobases on h-BN and Graphene: vdW Corrected DFT Calculations. *J. Phys. Chem. C* **2013**, *117*, 13435–13441.
41. Haskins, J.; Knac, A.; Sevik, C.; Sevinçli, H.; Cuniberti, G.; Çağın, T. Control of Thermal and Electronic Transport in Defect-Engineered Graphene Nanoribbons. *ACS Nano* **2011**, *5*, 3779–3787.
42. Diefenbach, M.; Kim, K. S. Towards Molecular Magnetic Switching with an Electric Bias. *Angew. Chem., Int. Ed.* **2007**, *46*, 7640–7643.
43. Datta, S. *Electronic Transport in Mesoscopic Systems*; Cambridge University Press: Cambridge, 1997.
44. Brandbyge, M.; Mozos, J.-L.; Ordejón, P.; Taylor, J.; Stokbro, K. Density-Functional Method for Nonequilibrium Electron Transport. *Phys. Rev. B* **2002**, *65*, 165401.
45. Taylor, J.; Guo, H.; Wang, J. *Ab Initio* Modeling of Quantum Transport Properties of Molecular Electronic Devices. *Phys. Rev. B* **2001**, *63*, 245407.
46. Perdew, J. P.; Zunger, A. Self-Interaction Correction to Density-Functional Approximations for Many-Electron Systems. *Phys. Rev. B* **1981**, *23*, 5048.
47. Troullier, N.; Martins, J. L. Efficient Pseudopotentials for Plane-Wave Calculations. *Phys. Rev. B* **1991**, *43*, 1993–2006.
48. Kim, W. Y.; Kim, K. S. Carbon Nanotube, Graphene, Nanowire, and Molecule-Based Electron and Spin Transport Phenomena Using the Nonequilibrium Green's Function Method at the Level of First Principles Theory. *J. Comput. Chem.* **2008**, *29*, 1073–1083.
49. Soler, J. M.; Artacho, E.; Gale, J. D.; García, A.; Junquera, J.; Ordejón, P.; Sánchez-Portal, D. The SIESTA Method for *ab Initio* Order-N Materials Simulation. *J. Phys.: Condens. Matter* **2002**, *14*, 2745–2779.
50. Lee, D. H.; Joannopoulos, J. D. Simple Scheme for Surface-Band Calculations. I. *Phys. Rev. B* **1981**, *23*, 4988–4996.